(4)

Graduate Aeronautical Laboratories
California Institute of Technology

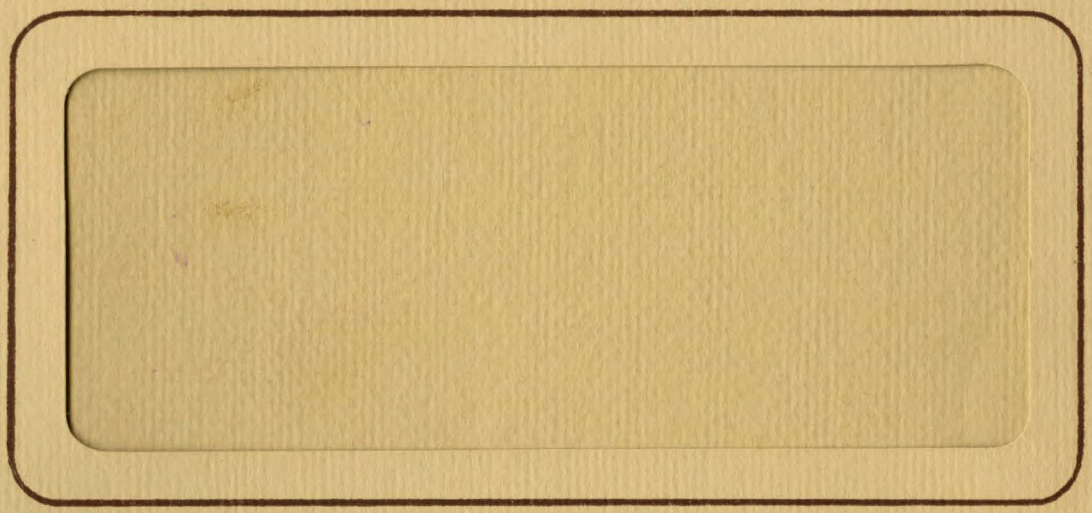

Firestone Flight Sciences Laboratory

Guggenheim Aeronautical Laboratory

Karman Laboratory of Fluid Mechanics and Jet Propulsion

Pasadena

GALCIT 118 A - PROGRESS REPORT NO. 4

Aerojet Contract S-420061-OP

February 28, 1962 - May 28, 1962

FUNDAMENTAL STUDIES RELATING TO THE MECHANICAL BEHAVIOR OF SOLID PROPELLANTS, ROCKET GRAINS AND ROCKET MOTORS

P. J. Blatz
W. L. Ko
A. R. Zak

GALCIT SM 62-23 May 1962

This program is being supported by the Aerojet-General Corporation, Sacramento Division, under technical cognizance of Dr. F. J. Climent to provide technical support to the Polaris Project

Firestone Flight Sciences Laboratory
California Institute of Technology
Pasadena, California

II. FRACTURE BEHAVIOR OF RUBBERY MATERIALS

A. INTRODUCTION

In the previous report the isothermal strain energy function and the associated constitutive stress and strain law for a 47 volume % voided polyurethane foam were presented. This function involves three parameters--the shear modulus, the f-factor, and the Blatz-Poisson ratio, all of which are constants of the material for deformations up to fracture. Based on experimental data obtained in three different stress fields, experimental values were assigned to each of these parameters. Some thought is being given to an analysis which will predict these parameters from a knowledge of the properties of the continuum binder and the void content and void size.

In addition, a failure criterion was proposed for this foam. In order to check further the invariance of the proposed criterion over the failure surface, additional data in a triaxial stress field were obtained. On the basis of these data and an inference based on thermodynamic consideration, which suggests that all carpets of the surface must be non-concave, it looks like the failure surface is the frustum of a triangular pyramid, the frustrated facet being the carpet of the hydrostatic plane. The sides of the frustum are then the carpets of the planes of maximum principal strain. Thus it looks like a dual criterion obtains: each criterion controls one of two subsets of failure modes.

In order to confirm the universality of the function, law and definition mentioned above, the triaxial tensile test was performed and reported in the previous report. Because of unsatisfactory bonding of the specimens, the test points were scattered around the theoretical curves.

The present report furnishes i) more triaxial data obtained with improved bonding of the specimens, and depicts more clearly the ii) failure surface based on the averaged experimental values of ultimate stresses in the normal stress space.

B. TRIAXIAL TENSION

$$\lambda_1 = \lambda \ , \qquad \lambda_2 = \lambda_3 = 1 \ , \qquad J_3 = \lambda \tag{II.1}$$

The constitutive stress-strain law becomes (cf. equation (I.5), Report No. 3):

$$\frac{\sigma_{tri}}{\mu} = \left[J_3^{\frac{2(1-\nu)}{1-2\nu}} - 1 \right]\left[f J_3^{-\frac{1}{1-2\nu}} + \frac{(1-f)}{J_3^3} \right] \qquad \text{(II.2)}$$

In this equation there are three unknown parameters, μ, ν, and f to be determined. In order to see how these appear in the triaxial tension, one must know any two of them in order to determine the third one. Hence we use the averaged shear modulus $\mu_{ave.}$ previously obtained from uniaxial and biaxial tensions, and thus determine the shear modulus fractional factor f by letting ν have the same value as the previous two kinds of tests, or determine ν by assuming the value of f based on previous tests.

Under such circumstances one can make two kinds of plots from (II.2), namely,

i) If f = 0, (II.2) yields,

$$\left[\frac{\sigma_{tri.}}{\mu_{ave.}} J_3^3 + 1 \right] = J_3^{\frac{2(1-\nu)}{1-2\nu}} \qquad \text{(II.3)}$$

and ν is determined from $\log\left[\frac{\sigma_{tri.}}{\mu_{ave.}} J_3^3 + 1\right]$ vs. $\log J_3$ plot whose slope is $\frac{2(1-\nu)}{1-2\nu}$ (cf. Fig. II.4) if the plot is a straight line.

ii) If $\nu = 1/4$, (II.2) yields,

$$\frac{\sigma_{tri.}}{\mu_{ave.}\left(J_3 - \frac{1}{J_3^2}\right)} = f + (1-f)\frac{1}{J_3} \qquad \text{(II.4)}$$

and f will be the intercept and (1-f) the slope provided the plot

$$\frac{\sigma_{tri.}}{\mu_{ave.}\left(J_3 - \frac{1}{J_3^2}\right)} \qquad \text{against} \qquad \frac{1}{J_3}$$

is a straight line (cf. Fig. II.5). The specimens used were, like before, 47% volume voids polyurethane foam of 1/4" thick with either 2 1/2" or 3" diameter. Eastman 910 adhesive was used for bonding the specimens to the plexiglass flanges (cf. Fig. II.1, Fig. II.2).

C. FAILURE SURFACE PLOT

The lateral stress in strip biaxial and triaxial tensions were calculated from equation (I.5), page 2, Report No. 3, which is repeated in the following:

$$\overline{\sigma}_i J_3 = \sigma_i \lambda_i = \mu f \left[\lambda_i^2 - J_3^{-\frac{2\nu}{1-2\nu}}\right] - \mu(1-f)\left[\frac{1}{\lambda_i^2} - J_3^{\frac{2\nu}{1-2\nu}}\right] \qquad (II.5)$$

and set $\nu = 1/4$, f = 0 then

$$\overline{\sigma}_i J_3 = \sigma_i \lambda_i = -\mu\left[\frac{1}{\lambda_i^2} - J_3\right] \qquad (II.6)$$

i) Strip biaxial tension: $\lambda_1 = \lambda$, $\lambda_2 = \lambda_{lat.} = 1$, $\lambda_3 = \lambda_{th.}$, $J_3 = \lambda\lambda_{th}$,

$$i = 2: \qquad \overline{\sigma}_{lat} = -\mu\left[\frac{1}{\lambda\lambda_{th.}} - 1\right] \qquad (II.7)$$

ii) Triaxial tension: $\lambda_1 = \lambda$, $\lambda_2 = \lambda_3 = 1$, $J_3 = \lambda$

$$i = 2 \text{ or } 3: \qquad \overline{\sigma}_{lat} = -\mu\left[\frac{1}{\lambda} - 1\right] \qquad (II.8)$$

All the measured and calculated true stresses are listed below.

	$\overline{\sigma}_1/\mu$	$\overline{\sigma}_2/\mu$	$\overline{\sigma}_3/\mu$
Uniaxial Tension	1.394	0	0
Strip-Biaxial Tension	0.838	0.322	0
Homogeneous-Biaxial Tension	0.556	0.556	0
Triaxial Tension	0.750	0.334	0.334

D. RESULTS AND DISCUSSION

The test points in Fig. II.5 scatter around the theoretical curve for which $\nu = 1/4$, f = 0, however, the test data in Fig. II.4 fall fairly close to the theoretical curve and, if the stress-extension curves in Fig. II.3 fall within a narrow band for far better bonding and less sample imperfections, one should expect a good agreement of theory and experiment. Thus one can say that the strain energy function, the associated stress-strain constitutive law being obtained so far and the definition of the large deformation Poisson's ratio are universal in any kind of stress fields.

The failure surface plotted generates a concave spherical surface with radius 2.5 times the magnitude of the ultimate uniaxial stress with center located in the first octane, at ($1.75\frac{\overline{\sigma}_{uni.}}{\mu}$, $1.75\frac{\overline{\sigma}_{uni.}}{\mu}$ $1.75\frac{\overline{\sigma}_{uni.}}{\mu}$) (cf. Fig. II.6). This is just a preliminary result obtained from the present available data and further investigation of the shape of the surface is required. Due to considerable stress concentration in biaxial tensions, the plot of these points make the line of intersection between the coordinate surface and the failure safe surface curved. But if the stress concentration is eliminated by improving the specimens geometry, it is expected that these curves will straighten out and that the actual surface is a plane whose normal is oriented at an angle $54^{o}44'$ to each of the coordinate axes, and the traces of which intersect the sides of a triangular pyramid. In order to determine the orientation of these sides, it is necessary to obtain failure data under superimposed hydrostatic pressure. This will be accomplished in the next six months.

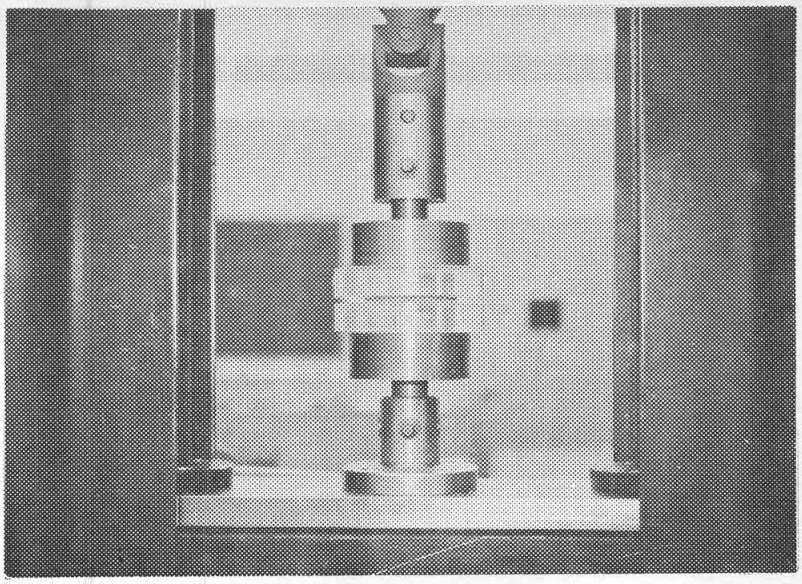

Fig. I. 1. Triaxial Tension at $\lambda = 1$

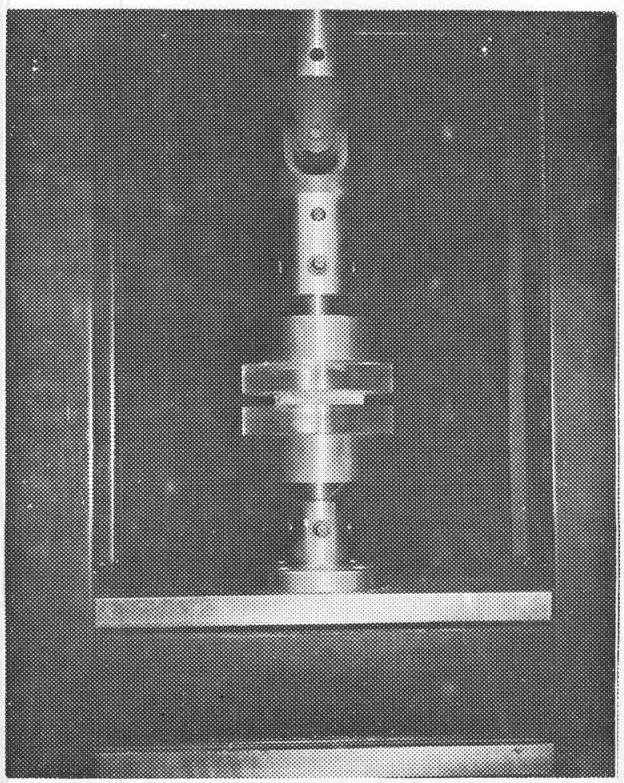

Fig. I. 2. Triaxial Tension at $\lambda = 2$

FIG. II.3. TRIAXIAL STRESS V.S. LONGITUDINAL EXTENTION RATIO

PU-FOAM (47% VOIDS)

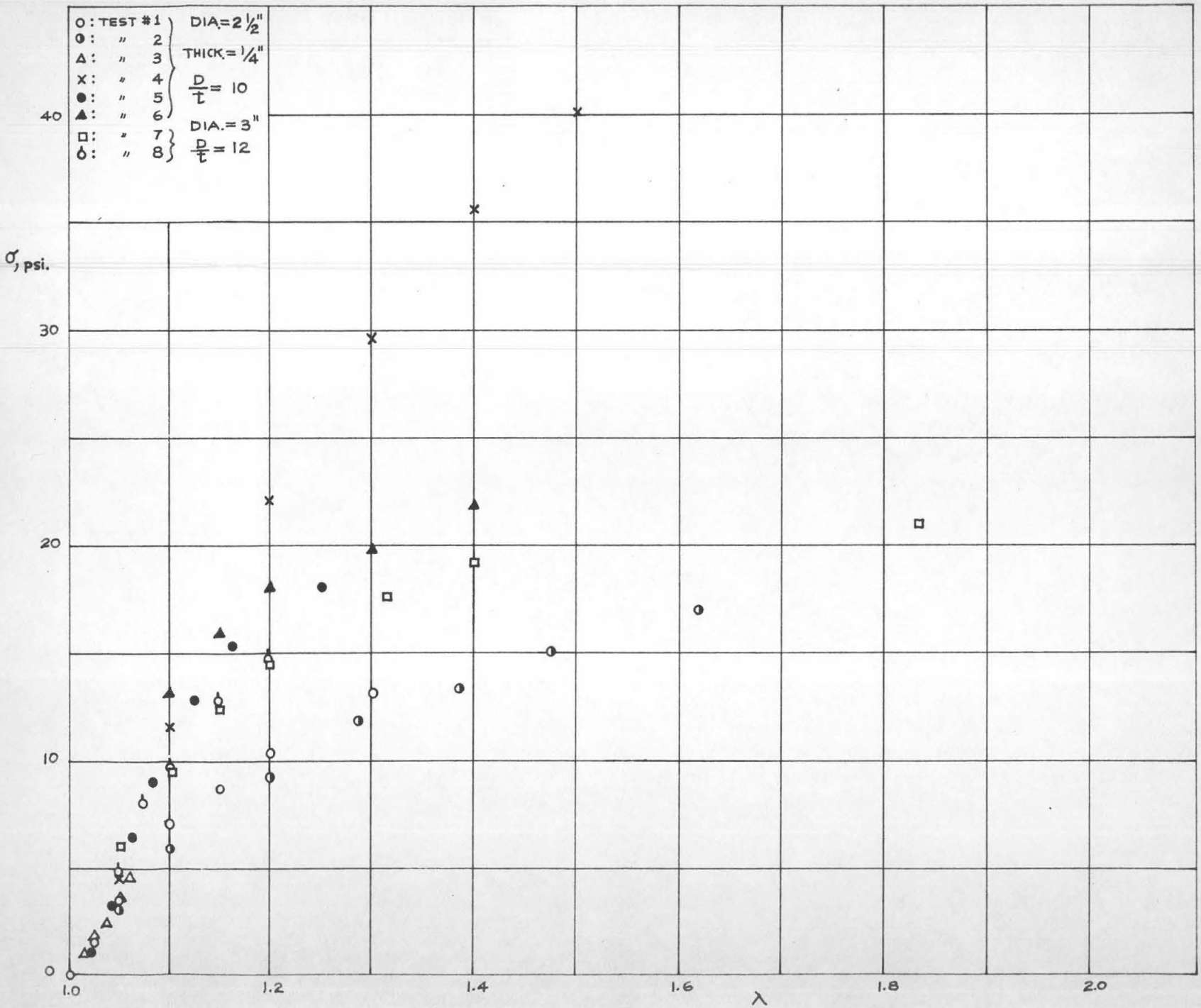

FIG. II. 4. EVALUATION OF ν FROM TRIAXIAL DATA. ASSUMPTION: $f = 0$, $\mu = \frac{1}{3}(\mu_{uni.} + \mu_{s\text{-}bi.} + \mu_{h\text{-}bi.}) = 32$ psi.

PU-FOAM (47% VOIDS)

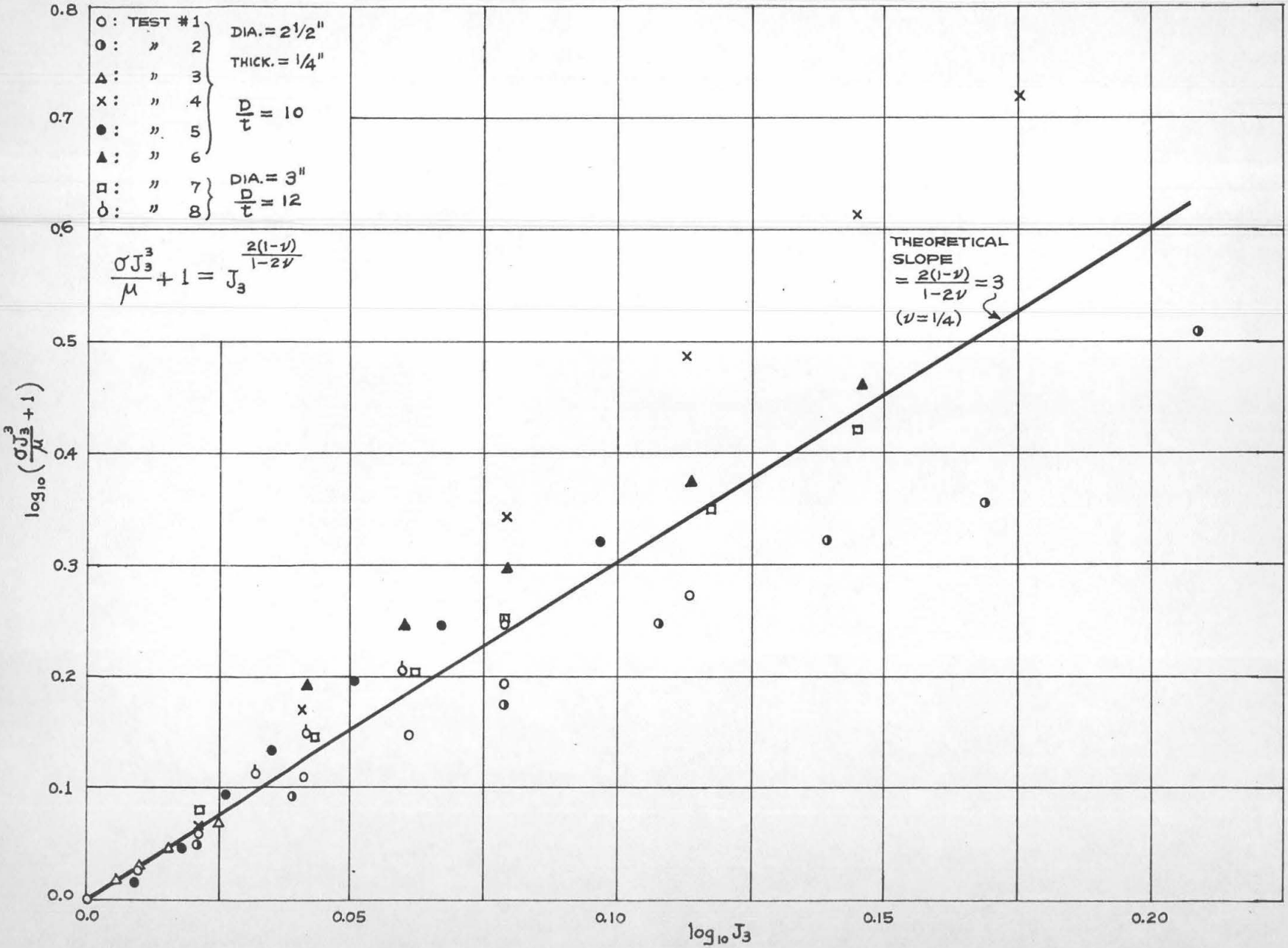

FIG. II.5. EVALUATION OF f FROM TRIAXIAL DATA. ASSUMPTION: $\nu = 1/4$, $\mu = \frac{1}{3}(\mu_{uni.} + \mu_{s\text{-}bi} + \mu_{h\text{-}bi}) = 32$ psi.

PU-FOAM (47% VOIDS)

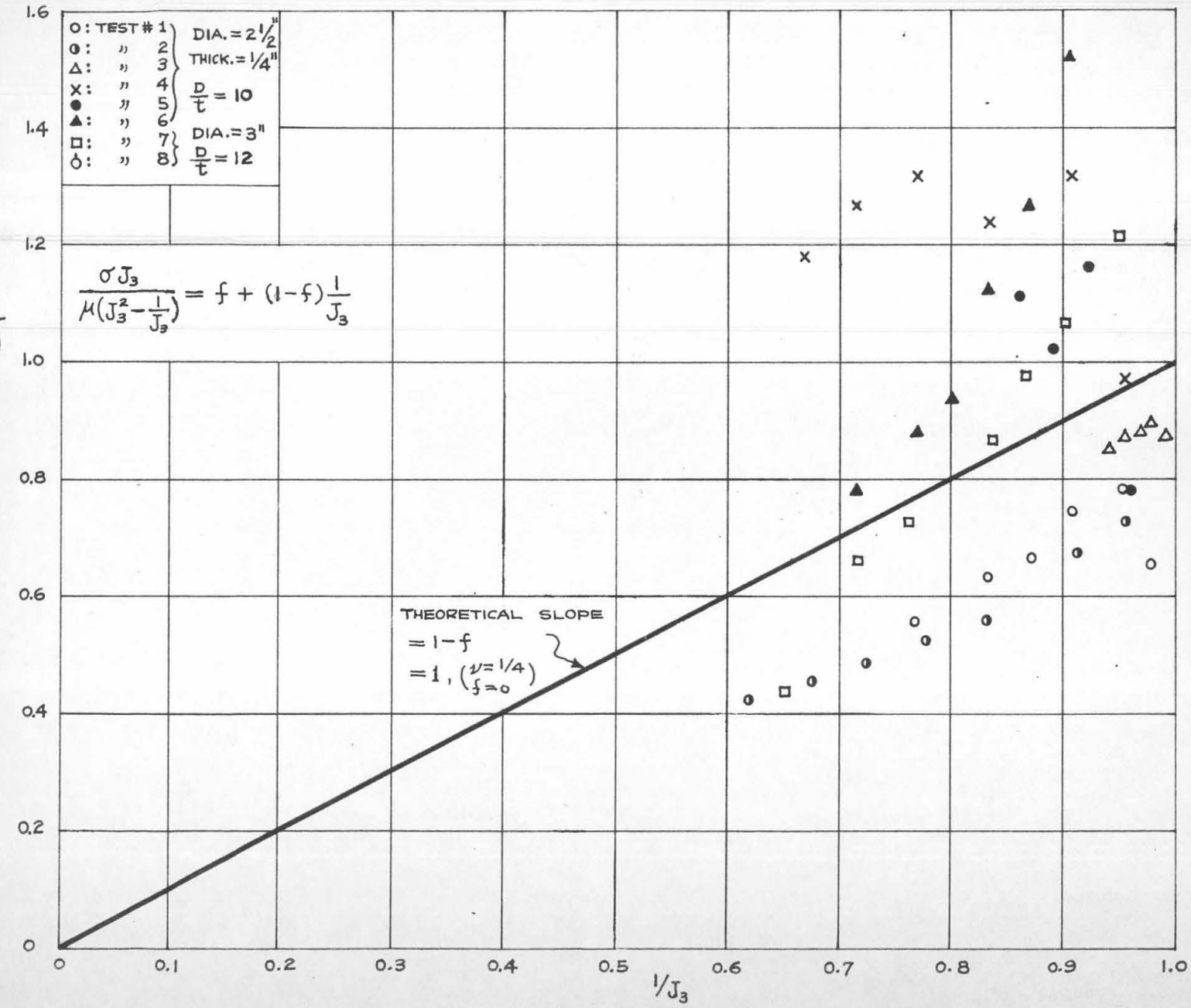

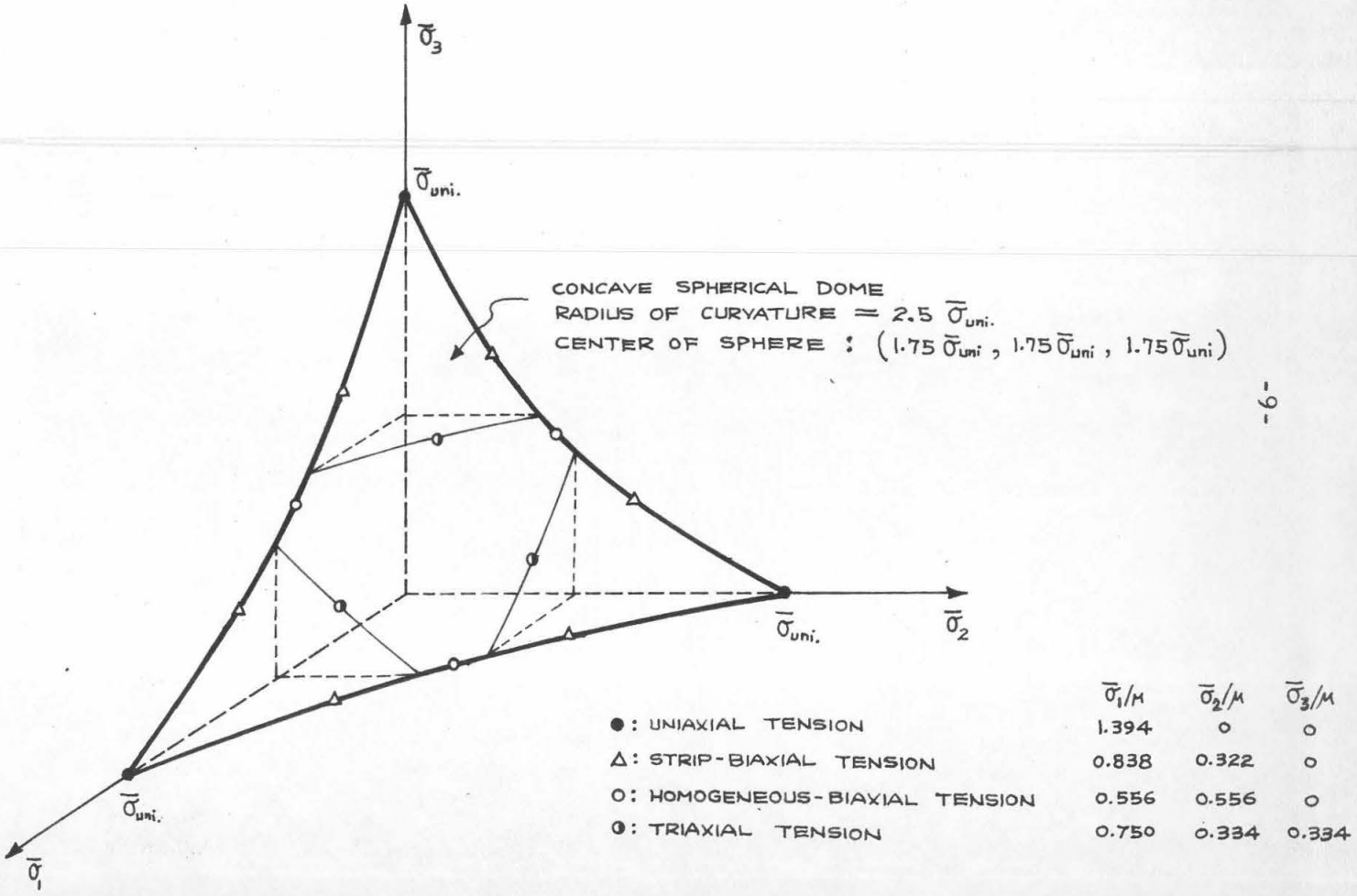

Fig. II.6. Failure Safe Surface Based on Experimental Data in Normal True Stress Space.

III. MOLECULAR STATISTICS

A. INTRODUCTION

Section I of this series of Progress Reports deals periodically with the phenomenological characterization of rubbery materials -- binders, foams, and filled foams, or propellants. Section II deals periodically with the strength characteristics of these materials. Because a knowledge of these characteristics is needed to predict the behavior of liners and propellants under conditions, it is important to place them on a scientific basis. In doing this, we correlate the phenomenological description of strength and small-strain response with the micro, and molecular description of the network and its chemical groupings, thereby providing information that the chemist needs to tailor organically "better" binders. Up to this period, the tool of molecular statistics has not been adduced, emphasis having been placed on determination of phenomenological description. In this and succeeding reports we will develop tools needed and carry out description in terms of molecular parameters.

In actuality, the term "molecular" at this point must be understood in a restricted sense. Because a typical network is an entangled mat of weakly interacting polymer chains, most of the mechanical properties of a binder (unfilled in this discussion) depend to a first-order approximation only on the topology and topography of these chains -- how long they are, how they are connected and entangled, how stiff or flexible they are, what is the concentration of juncture points and entanglements, where are the juncture points in space, are the entanglements mobile, are the entanglements single, multiple, or knotted loops. We hope to be able to shed light on all of these questions.

The first question we propose to discuss is that of the spatial distribution of juncture points. Since a binder cures statistically in the sense that the tri- or tetra-functional branching molecule enters the network in a random fashion (which is dictated primarily by its concentration relative to di-functional glycols, and which is conditioned somewhat by the relative reactive ratios of the various types of hydroxyl functions), it follows that the resulting branch - or juncture - points will be statistically distributed in space. We will restrict this discussion to

unfilled binders and therefore assume that this distribution spans a continuous space randomly. If this space is imagined sub-divided into tiny cells, then each cell will be seen to contain a small number of these branch points. We are interested in the following three questions: 1) What is the distribution of numbers of branch points per cell among the various cells which may be assumed to be labeled with respect to their spatial coordinates, 2) What is the distribution of the numbers of cells each having a specified number of branchpoints, 3) What is the spatial distribution of the branchpoints in any one cell as a function of the number of points in the cell. We shall develop the tools for this analysis.

The assumption of random distribution of branch points in space implies that some pairs of nearest neighbors are closer than others; this in turn implies that the chains joining neighbors need not all comprise the same given number of links. Indeed, as a result of what is learned by answering the questions posed above, we shall be able to delimit the question of how the chain lengths (measured in terms of numbers of linds or some such equivalent) are distributed. Finally we shall also be able to enforce some conditions upon the manner in which the chains are connected. This arises simply because the physical density of the binder is specified, and the binder is assumed to be a continuously connected body (no holes).

B. THE GRAND PARTITION FUNCTION

Consider a three-dimensional space divided up regularly into a finite number of small cubicles, the volume of which will be specified later. Sequentially these cubicles are labeled from 1 to N according to their respective positions in space, cf. two-dimensional sketch below.

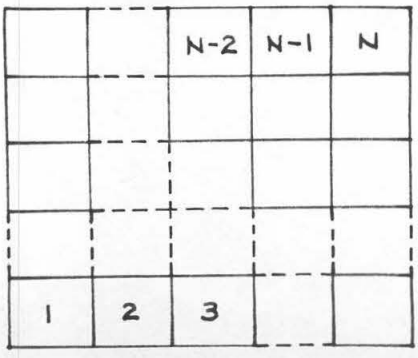

We are interested in how many ways a finite number M of branch points can be distributed among these cells. We are not concerned here with the specific location of the points in any one cell. Thus by "one way" is meant a particular set of numbers $\{Ms\}$, each of which specifies the number of branch points in a particular cell "s". "Two ways" are the same if and only if each number of the set $\{Ms\}$ is the same, in which case, all such "ways" contribute only one unit to the counting of the ways. Formally put, the number of ways is exactly the number of sets $\{Ms\}$ which satisfy the equation:

$$\sum_{S=1}^{N} M_s = M \qquad \text{(III. 1)}$$

Since the* $\{Ms\}$ is comprised of integers and is bounded by the lower value unity, and the upper value N, there is a finite number of solutions to the diophantine equation (III. 1). For example, when N = 2, and M = 10, possible solutions are : $\{1, 9\}$, $\{2, 8\}$, $\{3, 7\}$, $\{4, 6\}$ .... $\{8, 2\}$, $\{9, 1\}$. Note that $\{2, 8\}$ differs from $\{8, 2\}$ precisely because cell_1 is distinguished from cell_2 by their spatial coordinates.

We now ask for the probability associated with any one of these ways in the course of distributing the points among the cells. The a priori probability of finding a point in any given cell is defined by P_s, such that:

$$\sum_{S=1}^{N} P_s = 1 \qquad \text{(III. 2)}$$

The compound probability associated with the distribution of M points among N cells in a <u>given</u> order is then

* The word set will be ommitted from here on, since it is formally connoted by the brackets.

$$\prod_{s=1}^{N} p_s^{M_s} \tag{III. 3}$$

But, since the points are indistinguishable, the order in which they enter the cells is unimportant, and thus the factor (3) must be weighted by the number of orderings by which the M points can be distributed amont $\{Ms\}$; this is exactly

$$\frac{M!}{\prod_{s=1}^{N} M_s!} \tag{III. 4}$$

Thus the weighted probability associated with any one way is:

$$\Omega = M! \prod_{s=1}^{N} \frac{p_s^{M_s}}{M_s!} \tag{III. 5}$$

Obviously the sum of all these weighted probabilities must equal unity, We give this sum a special name -- the grand partition function -- and designate it by the symbol:

$$Z \equiv \sum_{\sum_1^N M_s = M} M! \prod_{s=1}^{N} \frac{p_s^{M_s}}{M_s!} \equiv \sum_{distr} \Omega = 1 \tag{III. 6}$$

Ths significance of this function will become clear after we have defined some of its properties.

1. The multinomial equivalence.

Consider the binomial expansion:

$$\left(\sum_{s=1}^{2} \chi_s\right)^N \equiv \sum_{k=0}^{M} \binom{M}{k} \chi_1^k \chi_2^{N-k} \qquad \text{(III. 7)}$$

The notation based on the symbol "k" is unwieldy because it is dissociated from the symbol "s". If however, we define: $k \equiv M_1$, and $N - k \equiv M_2$, we then have:

$$\left(\sum_{s=1}^{2} \chi_s\right)^M \equiv \sum_{\sum_{s=1}^{2} M_s = M} M! \prod_{s=1}^{2} \frac{\chi_s^{M_s}}{N_s!} \qquad \text{(III. 8)}$$

By induction, it follows that:

$$Z \equiv \sum_{\sum_{s=1}^{N} M_s = M} M! \prod_{s=1}^{N} \frac{P_s^{M_s}}{M_s!} \equiv \left(\sum_{s=1}^{N} P_s\right)^M = 1^M = 1 \qquad \text{(III. 9)}$$

Thus the grand partition function Z is equivalent to the M^{th} power of the sum of a priori probabilities, and is a fortiori equal to unity, when the a priori probabilities are normalized to unity. The sum $\sum_{1}^{N} P_s$ is termed the partition function and designated by the symbol q, so that:

$$Z = q^M \qquad \text{(III. 10)}$$

Incidentally, it is not necessary that q = 1, which in turn allows us to replace P_s by any analytic function of "s". We shall show later how this increases the efficacy of the grand partition function for diverse problems.

2. The grand average.

Since Z is a measure of the weighted probability of a given distribution of M points among N cells, averaged over all possible distributions ("ways"), it follows that any average property $\langle X_r \rangle$ of these distributions is given by:

$$\langle X_r \rangle = \frac{\sum_{\Sigma M_s = M} X_r \, M! \, \Pi \frac{P_s^{M_s}}{M_s!}}{\sum_{\Sigma M_s = M} M! \, \Pi \frac{P_s^{M_s}}{M_s!}} = \frac{\sum_{\text{distr}} X_r \, \Omega}{\sum_{\text{distr}} \Omega} \qquad \text{(III. 11)}$$

For example, if it is desired to know the average number of points $\langle M_r \rangle$, which one expects to find in a given cell "r", one can either compute it by means of (III. 11) or measure it by counting the actual number obtained in each of a very large number of actual distributions and then averaging over all these distributions. The computation goes as follows. In (III. 11), factor the r^{th} factor out of the product, designating the quotient with a prime:

$$\langle M_r \rangle = \frac{\sum_{\Sigma M_s = M} N_r \, M! \, \Pi' \frac{P_s^{M_s}}{M_s!} \frac{P_r^{M_r}}{M_r!}}{Z}$$

$$= \frac{M P_r \sum_{\Sigma M_s = M} (M-1) \, \Pi' \frac{P_s^{M_s}}{M_s!} \frac{P_r^{M_r - 1}}{(M_r - 1)!}}{Z} \qquad \text{(III. 12)}$$

Now let

$$\begin{aligned} M_1 &= M_1' \\ M_2 &= M_2' \\ &\cdots\cdots \\ M_r - 1 &= M_r' \\ &\cdots\cdots \\ &\text{etc.} \end{aligned} \qquad \text{(III. 13)}$$

Thus:

$$\langle M_r \rangle = \frac{M P_r \sum_{\Sigma M_s' = M-1} (M-1)! \, \Pi \frac{P_s^{M_s'}}{M_s'!}}{Z} = \frac{M P_r \left(\Sigma P_s \right)^{M-1}}{\left(\Sigma P_s \right)^{M}} = \frac{M P_r}{\Sigma P_s} \qquad \text{(III. 14)}$$

or

$$\frac{\langle M_r \rangle}{M} = \frac{P_r}{\sum P_s} \tag{III. 15}$$

Equation (III. 15) states the expected fractional number of points which locate in cell "r" is exactly equal to the fractional a priori probability of one point locating in that cell. Thus it follows that the $\{ p_r \}$ do not have to be normalized to unity, and therefore Z does not have to be restricted to probability considerations.

Furthermore, if all the a priori probabilities are equal,

$$P_r = \frac{1}{N} \tag{III. 16}$$

and

$$\langle M_r \rangle = \frac{M}{N} \tag{III. 17}$$

The results (III. 10) and (III. 17) are trivial in the sense that they flow immediately from the properties of Z. We shall how proceed to use Z to calculate another propertion of the distribution $\{M_s\}$ beside the mean $\langle M_r \rangle$.

3. The variance.

By definition, the variance of a distribution is given by:

$$\sigma_r^2 \equiv \langle (M_r - \langle M_r \rangle)^2 \rangle \tag{III. 18}$$

Since the averaging process is a linear operation, this can be put in the form:

$$\sigma_r^2 = \langle M_r (M_r - 1) \rangle + \langle M_r \rangle - \langle M_r \rangle^2 \tag{III. 19}$$

with

$$\langle M_r (M_r - 1) \rangle = \sum_{\Sigma M_s = M} M_r (M_r - 1)\, M! \prod \frac{P_s^{M_s}}{M_s!} \tag{III. 20}$$

Note that in (III. 19) the denominator does not appear on the right hand side, since it is equal to unity by (III. 9). The right hand side of (III. 20) is evaluated in the same way as (III. 12):

$$\langle M_r (M_r - 1) \rangle = \sum_{\Sigma M_s = M} M_r (M_r - 1)\, M! \prod{}' \frac{P_s^{M_s}}{M_s!} \frac{P_r^{M_r}}{M_r!} \tag{III. 21}$$

$$= M (M-1) P_r^2 \sum_{\Sigma M_s = M} (M-2)! \prod{}' \frac{P_s^{M_s}}{M_s!} \frac{P_r^{M_r - 2}}{(M_r - 2)!}$$

$$\langle M_r (M_r - 1) \rangle = M (M-1) P_r^2 \left(\sum P_s \right)^{M-2} = M (M-1) P_r^2 \tag{III. 22}$$

Equation (III. 19) becomes:

$$\sigma_r^2 = M P_r (1 - P_r) \tag{III. 23}$$

Since, in general, $p_r = 0\,(1/N) \ll 1$ (III. 24)

$$\sigma_r^2 \simeq M P_r = \langle M_r \rangle \tag{III. 25}$$

To a second order approximation, the distribution $\{M_r\}$ is Poisson, since the variance is very nearly equal the mean. We shall now display this statement more fully.

C. THE POISSON DISTRIBUTION

Consider now the second question: What is the distribution of numbers of cells $\{N_k\}$ each having a specified number of branchpoints "k"? We are interested first in the number of ways that N cells can be partitioned among an infinite number of classes labeled from k = 0 to k = ∞, subject to the restrictions that:

$$\sum_0^\infty N_k = N \tag{III. 26}$$

$$\sum_0^\infty k N_k = M \tag{III. 27}$$

Note first that, in practice, the upper limit of the summation variable "k" can never exceed N; formally, this is replaced by the statement that all $N_k = 0$, for $k > N$, i.e. -- there are no cells containing more than N branchpoints in any one distribution. Secondly, note that the number of solutions of the two linear diophantine equations (III. 26) and (III. 27) is less than those of (III. 1), and is in fact, a subset of the latter. Returning to

the previous example, with k = 1 or 2, N = 10, and adding the restriction that M = 16, we have only one possible solution $\{4, 6\}$. In the more general case in which the range of "k" is extended beyond two labelings, multiple solutions arise.

We now ask again for the probability associated with any one way of partitioning the N cells among classes labeled from k = 0 to k = ∞. This is equivalent to dismantling the cellular space, and dropping each cell that contains "k" branchpoints into a box labeled "k". The a priori probability of any one cell going into the proper box is thus unity, since no alternatives exist. The compound probability for putting all N cells into the boxes in any one <u>given</u> order is still unity. But since the cells are distinguishable, the order in which they enter the cells is important, and thus we seek a weighting factor, which is the number of orderings, keeping in mind that this must be independent of the ordering of the points in any one cell; this is exactly:

$$\Omega = \frac{N!}{\prod_{0}^{\infty} N_k! \, (k!)^{N_k}} \tag{III. 28}$$

The grand partition function which generates all these distributions is then:

$$Z = \sum_{\substack{\Sigma N_k = N \\ \Sigma k N_k = M}} \frac{N!}{\prod_{0}^{\infty} N_k! \, (k!)^{N_k}} = \sum_{(\text{distr})} \Omega \tag{III. 29}$$

The symbolism (distr) used in (III. 29) is to be interpreted as "all sets of solutions of (III. 26) and (III. 27); whereas the symbolism "distr" used in (III. 6) is to be interpreted as " all sets of solutions of (III. 1).

In order to evaluate (III. 29) , we rewrite it in the form:

$$Z = \text{Coeff. } z^M \left\{ \sum_{\Sigma N_k = N} N! \prod \frac{\left(\frac{z^k}{k!}\right)^{N_k}}{N_k!} \right\} \tag{III. 30}$$

This formalism both emphasizes the fact that $\{(\text{distr})\}$ is a subset of $\{\text{distr}\}$ and allows one to apply the multinominal equivalence to the complete set within the brackets of (III. 30):

$$Z = \text{Coeff. } z^M \left\{ \left(\sum_0^\infty \frac{z^k}{k!} \right)^N \right\} = \text{Coeff. } z^M \left\{ e^{N_z} \right\} = \frac{N^M}{M!} \tag{III. 31}$$

We are now in a position to evaluate the grand average number of cells expected in a given box "k":

$$\langle N_r \rangle = \frac{\text{Coeff. } z^M \left\{ \sum_{\Sigma N_k = N} N_r N! \prod \frac{\left(\frac{z^k}{k!}\right)^{N_k}}{N_k!} \right\}}{N^M/M!} \tag{III. 32}$$

which becomes after the usual manipulation:

$$\langle N_r \rangle = \frac{\frac{N}{r!} \text{Coeff. } z^{M-r} \left\{ \left(\sum_0^\infty \frac{z^k}{k!} \right)^{N-1} \right\}}{N^M/M!} = \frac{\frac{N}{r!} \frac{(N-1)^{M-r}}{(M-r)!}}{N^M/M!} \tag{III. 33}$$

or

$$\frac{\langle N_r \rangle}{N} = \binom{M}{r}\left(\frac{1}{N}\right)^r \left(1 - \frac{1}{N}\right)^{M-r} \qquad \text{(III. 34)}$$

This last result shows that the expected number of cells having "r" branchpoints is binomially distributed with respect to M and r, the a priori probability of an "r-type" occurrence being given by 1/N; this is equivalent to tossing M biased coins and asking for the probability that "r" heads will appear, if the a priori probability of a head is 1/N, a small number. It is well known that such a skewed binomial distribution is exactly, in the limit of infinitely large M and N, a Poisson distribution. To see this, expand the right hand side of (III. 34) by Stirling's approximation subject to the assumption that M/N remains finite and $r << M$:

$$\frac{\langle N_r \rangle}{N} \simeq \frac{\left(\frac{M}{N}\right)^r e^{-\frac{M}{N}}}{r!} \qquad \text{(III. 35)}$$

This distribution satisfies (III. 26) and (III. 27), as does (III. 34), and in addition has the following properties:

1. The maximum term occurs when $r_* = M/N$, which is the characteristic parameter of the distribution.

2. The mean $\langle r \rangle$ generated by this distribution is

$$\langle r \rangle = \sum_0^\infty r \left(\frac{M}{N}\right) \frac{e^{-\frac{M}{N}}}{r!} = \frac{M}{N} \qquad \text{(III. 36)}$$

3. The variance σ_r^2 generated by this distribution is:

$$\sigma_r^2 = \sum_0^\infty \left(r - \frac{M}{N}\right)^2 \left(\frac{M}{N}\right)^r \frac{e^{-\frac{M}{N}}}{r!} = \frac{M}{N} \qquad \text{(III. 37)}$$

These are very nearly the results obtained in (III. 25) and thus the distribution (III. 35) is an excellent replacement for the distribution (III. 15). In fact, (III. 34) is the exact replacement. It has the following properties:

1. The maximum term occurs when $r_* = M/N$, although the distribution is based on the two separate parameters M and N.
2. The mean $\langle r \rangle$ generated by this distribution is: $\langle r \rangle = M/N$, which follows from (III. 27)
3. The variance σ_r^2 generated by this distribution is:

$$\sigma_r^2 = \frac{M}{N}\left(1 - \frac{M}{N}\right) \qquad \text{(III. 38)}$$

These are exactly the results obtained in (III. 25).

D. THE RADIAL DISTRIBUTION FUNCTION

The third question has to do with the spatial distribution of the branchpoints. The tools developed in paragraphs A B C of this section enable us to answer this question in part. An alternative but complementary treatment will be presented in next month's report.

The term radial distribution refers to the number distribution of branchpoints relative to the radial distance measured from some arbitrary but fixed point in space. For convenience, we assume this point to be surrounded by a regularly spaced sequence of concentric spherical shells of radii; a, 2a, 3a, etc. Then the a priori probability of locating a point between $[(s-1)a]$ and (sa) is conveniently measured by the fractional volume of the annular cell contained between these two shells relative to the volume enclosed by the N^{th} cell:

$$p_s = \frac{s^3 - (s-1)^3}{N^3} = \frac{\Delta(s^3)}{N^3} \qquad \text{(III. 39)}$$

Note that these probabilities are normalized to unity. By (III. 15), the fractional number of points between shells (s -1) and s is simply:

$$\frac{\langle M_s \rangle}{M} = \frac{\Delta s^3}{N^3} \qquad \text{(III. 40)}$$

For small s, expression (III. 40) behaves like $1/N^3$, whereas, for large s,

$$\frac{\langle M_s \rangle}{M} \simeq \frac{3 s^2 \Delta s}{N^3} = O\left(\frac{1}{N}\right) \qquad \text{(III. 41)}$$

Thus the radial distribution of points (assuming isotropy, of course) increases rapidly like a quadratic function. In the next report, we shall introduce quantitative limits for the cell sizes associated with small numbers (10 - 100) of branchpoints, and then go on to determine the influence of the distribution of these points upon the chain-length distribution.

IV. STRESS ANALYSIS

A. STRESS SINGULARITIES IN CYLINDRICAL BODIES CONTINUED

1. Introduction

In the Progress Report No. 3 a method was presented for investigating the stress singularities in the neighborhood of boundary discontinuities in cylindrical bodies. The general problem was formulated in terms of a stress function F and a solution for this function was obtained in the form

$$F = \rho^{\lambda+1}\left[a\sin(\lambda+1)\phi + b\cos(\lambda+1)\phi + c\sin(\lambda-1)\phi + d\cos(\lambda-1)\phi\right] \quad \text{(IV.1)}$$

This solution was then used to analyze stress singularities in two specific configurations which were designated by Case I and Case II.

Since the publication of the Progress Report No. 3 the investigation in this area has continued and the results obtained during this investigation will be presented in this part of the present report. As part of the investigation Case I and Case II of the previous report will be reworked since an algebraic error in the previous report has been discovered. Therefore pages 36 to 41 of Progress Report No. 3 are to be disregarded.

2. The analysis

The stresses and displacements are related to the stress function by eqs. (IV.33) and (IV.34) of the previous report. For the purpoase of the present analysis, and for future reference, it is useful to transform these expressions from the cylindrical coordinate system r, z to the new coordinates ρ , ϕ which have already been defined. This has been done and the results, written in terms of the solution for the stress function F from eq. (IV.1), have the form

$$\frac{\sigma_r}{(\lambda-1)\lambda} = \rho^{\lambda-2}\Big\{a(\lambda+1)\sin(\lambda-2)\phi + b(\lambda+1)\cos(\lambda-2)\phi$$

$$+c\left[(-1+4\nu)\sin(\lambda-2)\phi + (\lambda-2)\sin(\lambda-4)\phi\right]$$

$$+d\left[(-1+4\nu)\cos(\lambda-2)\phi + (\lambda-2)\cos(\lambda-4)\phi\right]\Big\} \quad \text{(IV.2)}$$

$$\frac{\sigma_\theta}{(\lambda-1)\lambda} = \rho^{\lambda-2}\{ c\,4\nu\sin(\lambda-2)\phi + d\,4\nu\cos(\lambda-2)\phi \} \tag{IV.3}$$

$$\begin{aligned}\frac{\sigma_3}{(\lambda-1)\lambda} = \rho^{\lambda-2}\{ & -a(\lambda+1)\sin(\lambda-2)\phi - b(\lambda+1)\cos(\lambda-2)\phi \\ & + c[(5-4\nu)\sin(\lambda-2)\phi - (\lambda-2)\sin(\lambda-4)\phi] \\ & + d[(5-4\nu)\cos(\lambda-2)\phi - (\lambda-2)\cos(\lambda-4)\phi]\}\end{aligned} \tag{IV.4}$$

$$\begin{aligned}\frac{\tau_{r3}}{(\lambda-1)\lambda} = \rho^{\lambda-2}\{ & a(\lambda+1)\cos(\lambda-2)\phi - b(\lambda+1)\sin(\lambda-2)\phi \\ & + c[(-3+4\nu)\cos(\lambda-2)\phi + (\lambda-2)\cos(\lambda-4)\phi] \\ & + d[(3-4\nu)\sin(\lambda-2)\phi + (-\lambda+2)\sin(\lambda-4)\phi]\}\end{aligned} \tag{IV.5}$$

The displacements are

$$\begin{aligned}\frac{uE}{(1+\nu)\lambda} = \rho^{\lambda-1}\{ & a(\lambda+1)\cos(\lambda-1)\phi - b(\lambda+1)\sin(\lambda-1)\phi \\ & + c(\lambda-1)\cos(\lambda-3)\phi - d(\lambda-1)\sin(\lambda-3)\phi\}\end{aligned} \tag{IV.6}$$

$$\begin{aligned}\frac{wE}{(1+\nu)\lambda} = \rho^{\lambda-1}\{ & -a(\lambda+1)\sin(\lambda-1)\phi - b(\lambda+1)\cos(\lambda-1)\phi \\ & + c[(6-8\nu)\sin(\lambda-1)\phi - (\lambda-1)\sin(\lambda-3)\phi] \\ & + d[(6-8\nu)\cos(\lambda-1)\phi - (\lambda-1)\cos(\lambda-3)\phi]\}\end{aligned} \tag{IV.7}$$

3. Elastic body bounded by $\phi = 0$ and $\phi = \frac{\pi}{2}$.

This corresponds to a right angle cylinder and we shall investigate four different sets of boundary conditions. These are, at $\phi = 0$ and $\phi = \frac{\pi}{2}$ respectively: free-free, free-clamped, clamped-free, and clamped-clamped. The second and third set of conditions correspond, of course, to Case I and Case II of the previous report.

For the free-free case the boundary conditions are, at $\phi = 0$

$$\sigma_r = \tau_{rz} = 0 \tag{IV.8}$$

and at $\phi = \frac{\pi}{2}$

$$\sigma_z = \tau_{rz} = 0 \tag{IV.9}$$

Using eqs. (IV.2), (IV.4) and (IV.5) the above boundary conditions lead to the following homogeneous algebraic equations

$$b(\lambda+1) + d(\lambda - 3 + 4\nu) = 0 \tag{IV.10a}$$

$$a(\lambda+1) + c(\lambda - 5 + 4\nu) = 0 \tag{IV.10b}$$

$$a(\lambda+1)\sin\lambda\tfrac{\pi}{2} + b(\lambda+1)\cos\lambda\tfrac{\pi}{2} - c(\lambda+3-4\nu)\sin\lambda\tfrac{\pi}{2} + d(\lambda+3-4\nu)\cos\lambda\tfrac{\pi}{2} = 0 \tag{IV.10c}$$

$$-a(\lambda+1)\cos\lambda\tfrac{\pi}{2} + b(\lambda+1)\sin\lambda\tfrac{\pi}{2} + c(\lambda+1-4\nu)\cos\lambda\tfrac{\pi}{2} - d(\lambda+1-4\nu)\sin\lambda\tfrac{\pi}{2} = 0 \tag{IV.10d}$$

For a non-trivial solution to exist for eqs. (IV.10) the determinant of the coefficients of a, b, c, and d has to vanish. This leads to a characteristic equation in the unknown parameter λ ,

$$\lambda^2 - 2\lambda + 1 - \cos^2\lambda\tfrac{\pi}{2} = 0 \tag{IV.11}$$

For the free-clamped case the boundary conditions are,

$$\text{at } \phi = 0, \qquad \sigma_z = \tau_{rz} = 0 \tag{IV.12}$$

$$\text{and at } \phi = \frac{\pi}{2}, \qquad u = w = 0 \tag{IV.13}$$

Using eqs. (IV.2), (IV.5), (IV.6), and (IV.7) the above boundary conditions generate the following algebraic equations

$$b(\lambda+1) + d(\lambda - 3 + 4\nu) = 0 \tag{IV.14a}$$

$$a(\lambda+1) + c(\lambda - 5 + 4\nu) = 0 \tag{IV.14b}$$

$$-a(\lambda+1)\sin\lambda\frac{\pi}{2} - b(\lambda+1)\cos\lambda\frac{\pi}{2} + c(\lambda-1)\sin\lambda\frac{\pi}{2} + d(\lambda-1)\cos\lambda\frac{\pi}{2} = 0 \tag{IV.14c}$$

$$a(\lambda+1)\cos\lambda\frac{\pi}{2} - b(\lambda+1)\sin\lambda\frac{\pi}{2} - c(\lambda+5-8\nu)\cos\lambda\frac{\pi}{2} + d(\lambda+5-8\nu)\sin\lambda\frac{\pi}{2} = 0 \tag{IV.14d}$$

The characteristic equation corresponding to eqs. (IV.14) is

$$\lambda^2 - 2\lambda - 3 + 8\nu - 4\nu^2 + (3-4\nu)\cos^2\lambda\frac{\pi}{2} = 0 \tag{IV.15}$$

For the clamped-free conditions the boundary conditions are,

$$\text{at } \phi = 0, \qquad u = w = 0 \tag{IV.16}$$

$$\text{and at } \phi = \frac{\pi}{2}, \qquad \sigma_z = \tau_{rz} = 0 \tag{IV.17}$$

Using eqs. (IV.6), (IV.7), (IV.4) and (IV.5) the above boundary conditions produce the following algebraic equations

$$a(\lambda+1) + c(\lambda-1) = 0 \tag{IV.18a}$$

$$b(\lambda+1) + d(\lambda-7+8\nu) = 0 \tag{IV.18b}$$

$$a(\lambda+1)\sin\lambda\tfrac{\pi}{2} + b(\lambda+1)\cos\lambda\tfrac{\pi}{2} - c(\lambda+3-4\nu)\sin\lambda\tfrac{\pi}{2} - d(\lambda+3-4\nu)\cos\lambda\tfrac{\pi}{2} = 0 \tag{IV.18c}$$

$$-a(\lambda+1)\cos\lambda\tfrac{\pi}{2} + b(\lambda+1)\sin\lambda\tfrac{\pi}{2} + c(\lambda+1-4\nu)\cos\lambda\tfrac{\pi}{2} - d(\lambda+1-4\nu)\sin\lambda\tfrac{\pi}{2} = 0 \tag{IV.18d}$$

The corresponding characteristic equation is

$$\lambda^2 - 2\lambda - \beta + 8\nu - 4\nu^2 + (3-4\nu)\cos^2\lambda\tfrac{\pi}{2} = 0 \tag{IV.19}$$

It is interesting to note that equation (IV.19) is exactly the same as (IV.15); therefore it can be immediately deduced that the eigen values λ will be the same for the free-clamped and the clamped-free case.

For the clamped-clamped case the boundary conditions are,

$$\text{at } \phi = 0, \qquad u = w = 0 \tag{IV.20}$$

$$\text{and at } \phi = \tfrac{\pi}{2}, \quad u = w = 0 \tag{IV.21}$$

and the corresponding algebraic equations, from (IV.6) and (IV.7), are

$$a(\lambda+1) + c(\lambda-1) = 0 \tag{IV.22a}$$

$$b(\lambda+1) + d(\lambda-7+8\nu) = 0 \tag{IV.22b}$$

$$-a(\lambda+1)\sin\lambda\tfrac{\pi}{2} - b(\lambda+1)\cos\lambda\tfrac{\pi}{2} + c(\lambda-1)\sin\lambda\tfrac{\pi}{2} + d(\lambda-1)\cos\lambda\tfrac{\pi}{2} = 0 \tag{IV.22c}$$

$$a(\lambda+1)\cos\lambda\tfrac{\pi}{2} - b(\lambda+1)\sin\lambda\tfrac{\pi}{2} - c(\lambda+5-8\nu)\cos\lambda\tfrac{\pi}{2} + d(\lambda+5-8\nu)\sin\lambda\tfrac{\pi}{2} = 0 \qquad \text{(IV.22d)}$$

The corresponding characteristic equation is

$$\lambda^2 - 2\lambda + 1 + (-9 + 24\nu - 16\nu^2)\cos^2\lambda\tfrac{\pi}{2} = 0 \qquad \text{(IV.23)}$$

The discussion of the four characteristic equations which have been obtained above is postponed to the end for the section and we now proceed to the next configuration.

4. Elastic body bounded by $\phi = 0$ and $\phi = \pi$.

This case corresponds to a cylinder without geometrical discontinuities. We shall again investigate the four different sets of boundary conditions: free-free, free-clamped, clamped-free, and clamped-clamped, at $\phi = 0$ and $\phi = \pi$ respectively.

For the sake of brevity only the resulting characteristic equations will be given for this configuration. The corresponding algebraic expressions between a, b, c and d can be obtained, if desired, with a small amount of effort by using the appropriate equations for stresses and displacements and satisfying the appropriate boundary conditions.

For the free-free and the clamped-clamped cases the characteristic equations are the same:

$$\sin\lambda\pi = 0 \qquad \text{(IV.24)}$$

For the free-clamped and the clamped-free case the characteristic equation is

$$(1-2\nu)^2 + (3-4\nu)\cos^2\lambda\pi = 0 \qquad \text{(IV.25)}$$

5. Elastic body bounded by $\phi = 0$ and $\phi = 2\pi$.

This case corresponds to a crack which has a cylindrical shape. Again the four different sets of boundary conditions have been investigated

and the characteristic equations obtained.

For the free-free and clamped-clamped case the characteristic equation is

$$\sin \lambda 2\pi = 0 \tag{IV.26}$$

And for the free-clamped and clamped-free case the corresponding equation is

$$(1-2\nu)^2 + (3-4\nu)\cos^2 \lambda 2\pi = 0 \tag{IV.27}$$

6. Discussion of results.

For a reason which shall become obvious later in the discussion, a new variable λ' is introduced. This new variable is defined by

$$\lambda' = \lambda - 1 \tag{IV.28}$$

With this new variable the characteristic equations, which were obtained above, are tabulated for easy reference in Table 1 on the following page. By comparing the characteristic equations in Table 1 with the results obtained by Williams* it is obvious that these equations are the same as the ones pertaining to an infinite wedge under plain strain conditions. In this comparison the total angle of the cylindrical body has to be compared to the total angle of the corresponding wedge. In the present analysis the stresses are proportional to $\rho^{\lambda'-1}$ and in the wedge analysis by Williams the stresses are proportional to $\rho^{\lambda-1}$ where λ in that analysis has the one to one correspondence to λ' in the characteristic equations. Therefore the solution for the cylindrical bodies, which have been examined in the present analysis, are governed by the same eigen values as are the infinite wedge bodies under conditions of plain strain. Whether such a result is true for a general cylindrical body, bounded by any two arbitrary angles, has not yet been determined. However an analysis is at present being carried out to answer this question,

---

*Williams, M. L., "Stress Singularities Resulting from Various Boundary Conditions in Angular Corners of Plates in Extension", J. App. Mech. Dec. 1952, p. 526.

Body Bounded by the Angles	Boundary Conditions	Characteristic Equation
$\phi = 0$ and $\phi = \frac{\pi}{2}$	free-free	$\sin \lambda' \frac{\pi}{2} = \pm \lambda'$
	free-clamped clamped-free	$\sin^2 \lambda' \frac{\pi}{2} + \frac{4(1-\nu)^2}{3-4\nu} = \left(\frac{\lambda'}{3-4\nu}\right)^2$
	clamped-clamped	$\sin^2 \lambda' \frac{\pi}{2} = \left(\frac{\lambda'}{3-4\nu}\right)^2$
$\phi = 0$ and $\phi = \pi$	free-free clamped-clamped	$\sin \lambda' \pi = 0$
	free-clamped clamped-free	$\sin^2 \lambda' \pi = \frac{4(1-\nu)^2}{3-4\nu}$
$\phi = 0$ and $\phi = 2\pi$	free-free clamped-clamped	$\sin \lambda' 2\pi = 0$
	free-clamped clamped-free	$\sin^2 \lambda' 2\pi = \frac{4(1-\nu)^2}{3-4\nu}$

Table 1. Characteristic Equations

the outcome of this analysis will be presented in the next report.

The solution to the characteristic equations may in general be complex. It can quickly be seen that three of the equations in Table 1 have completely real solutions; the remaining ones have one real and an infinite number of complex solutions. All of these latter equations are similar in form to eq. (IV.18) on page 21 of Progress Report No. 3. That particular equation arose when the Mellin Integral Transform method was used to solve the problem for an infinite wedge. A systematic method for finding all the solutions to such an equation was presented in the previous report and it will not be repeated here.

The present analysis can be used to obtain stress distribution in the neighborhood stress singularity points. In the case when a singularity in the stress exists, the eigen value, and therefore the corresponding eigen function, which produces this singularity, is the predominant one in the neighborhood of the singularity. Therefore for any configuration having determined the value of this eigen value the eigen function can be also determined, up to one multiplying constant, by using the algebraic equations corresponding to the appropriate boundary conditions. Having determined this function the stresses at any point in the body in the neighborhood of the singularity can be calculated using eqs. (IV.2), (IV.3), (IV.4) or (IV.5). The unknown multiplying constant has to be determined from overall stress conditions. Such an approach will be illustrated in the next report.

B. FURTHER CONSIDERATIONS OF THE SLUMP PROBLEM

1. Vertical slump

It is readily shown* that the axial slump of an infinitely long hollow cylindrical grain of elastic material encased in a rigid metal shell and subjected to Ng's of vertical acceleration produces a stress field in which all normal components are zero, and in which the shear stress is given by:

* Williams, M.L.; Blatz, P.J.; Schapery, R.A.: "Fundamental Studies Relating to Systems Analysis of Solid Propellants," GALCIT SM 61-5, California Institute of Technology, February 1961, p. 159.

$$\tau_{rz} = \frac{N\rho g}{2}\left(r - \frac{a^2}{r}\right) \qquad \text{(IV.29)}$$

where a is the inner radius of the propellant shell. Furthermore, since there are no normal stresses, the normal strains are zero regardless of the anisotropic nature of the material. As a result the vertical displacement depends only on the shear modulus of the material. From (IV.30) one can estimate an upper diameter (IV.31) to a vertically accelerating shell, assuming that a maximum shear stress can be accommodated by the adhesion at the propellant-case interface. For a cross-section (a_f) loading of 80 percent, with ρ = 0.0625 lbm/cu in, and $\tau_{rz} \leq$ 100 psi, we have:

$$\tau_{rz} = \frac{N\rho g b}{2}\left(\frac{b^2 - a^2}{b^2}\right) = \frac{N\rho g b}{2} a_f \qquad \text{(IV.30)}$$

$$2b = \frac{4\tau_{rz}}{N\rho g a_f} \doteq 667 \text{ ft/g} \qquad \text{(IV.31)}$$

Thus adhesive shear stress is not a limiting factor.

On the other hand, a non-idealized rocket motor is finite in length and is supported at either end by fore-and-aft-caps. The effect of these structures is to decrease the shear stress and increase the normal tear stress. A critical evaluation of this stress is better provided by the study of horizontal slump, in which the cylinder is deformed out-of-round.

2. Horizontal slump

The case of horizontal slump of an isotropic circularly perforated grain bonded to a rigid metal case was first studied by Lianis*. Unfortunately an error in the sign of the second term on the right hand side of his equation (3.10) has been propagated throughout his report resulting in incorrect values of the constants of the solution. The corrected solution will be presented below.

---

* Analysis of Deformation of Viscoelastic Bodies Due to Graviational Forces, Report No. S-60-1, School of Aeronautics and Engineering, Purdue University, Lafayette, Indiana, June 1960.

In addition to considering uniform horizontal slump in a rigid case, one should perhaps devote attention to the problem of non-uniform horizontal slump in an elastic case supported by periodic stiffeners. The solution in this problem, although extremely more difficult in nature, could provide a more realistic evaluation of the effects of slump than that presented below. It is not planned to discuss this problem in the near future, however, since it will be shown that the stresses and strains which result in the case of uniform slump are so small that even a one-order-of-magnitude increase introduced by non-uniformity would not suffice to render slump a serious problem.

In carrying out the plane strain analysis of horizontal slump, it was assumed that the propellant behaved isotropically in order to avoid extreme algebraic complexities. The usefulness of the conclusion drawn under this restrictive assumption is not vitiated, since an anisotropic analysis based on the considerations of the previous section, can only decrease the stresses, presumably by less than one order of magnitude.

Before presenting the details of the analysis, the form of the stresses and displacements is displayed. Taking $\theta = 0$ in the horizontal direction,

$$\sigma_r = \left(\delta + 2iC + \frac{(8\nu-3)iB}{r} + \frac{2iF}{r^3}\right)\sin\theta \qquad \text{(IV.32)}$$

$$\sigma_\theta = \left(\delta + 2iC + \frac{(9-8\nu)iB}{r} - \frac{2iF}{r^3}\right)\sin\theta \qquad \text{(IV.33)}$$

$$\tau_{r\theta} = -2i\left(Cr + \frac{B(1-2\nu)}{r} - \frac{F}{r^3}\right)\cos\theta \qquad \text{(IV.34)}$$

$$2\mu u_r = \left\{\left[(3-4\nu)A - \bar{D}\right] + B + 2(3-4\nu)B\ln r + 2Cr^2 + \frac{F}{r^2} + \left[(3-4\nu)C - \frac{i\delta}{2}(1-2\nu)r^2\right]\right\}\cos\theta \qquad \text{(IV.35)}$$

$$2\mu u_\theta = \left\{-\left[(3-4\nu)A - \bar{D}\right] + B - 2(3-4\nu)B\ln r - 2Cr^2 + \frac{F}{r^2} + \left[(3-4\nu)C - \frac{i\delta}{2}(1-2\nu)r^2\right]\right\}\sin\theta \qquad \text{(IV.36)}$$

where A, B, C, $\overline{D}$, F are imaginary constants which depend only on the specific weight of the propellant, the grain geometry, and Poisson's ratio.

The solution to this problem is expedited tremendously by the use of complex variable techniques. Thus the circular ring of propellant is geometrized as an annulus on the complex plane; the gravity vector acts in the minus "i" direction. The polar coordinates in real space are represented on the field of complex numbers by the relations:

$$z = r e^{i\theta} \tag{IV.37}$$

$$\bar{z} = r e^{-i\theta} \tag{IV.38}$$

The equilibrium equations in polar coordinates are given by:

$$r \frac{\partial \sigma_r}{\partial r} + \sigma_r - \sigma_\theta + \frac{\partial \tau_{r\theta}}{\partial \theta} = \delta r \sin\theta \tag{IV.39}$$

$$r \frac{\partial \tau_{r\theta}}{\partial r} + 2\tau_{r\theta} + \frac{\partial \sigma_\theta}{\partial \theta} = \delta r \cos\theta \tag{IV.40}$$

where

$$\delta = \rho g \tag{IV.41}$$

represents the body force per unit volume of propellant.

We now introduce the complex stresses and displacement:

$$s = \sigma_r + \sigma_\theta \tag{IV.42}$$

$$2t = \sigma_r - \sigma_\theta + 2i\tau_{r\theta} \tag{IV.43}$$

$$u = u_r + i u_\theta \tag{IV.44}$$

Using the new variables $z, \bar{z}$, equations (IV.39), (IV.40) with (IV.42) to (IV.44) become:

$$\bar{z} s_{\bar{z}} + 2 z t_z + 2t = i\delta \bar{z} \tag{IV.45}$$

Note that only one complex equation is needed to represent two real equations, since the complex equation can always be separated. The subscripts indicate partial differentiation with respect to z or $\bar{z}$. The new equilibrium equation (IV.45) is satisfied identically by stresses

derived from a generating function $\bar{\Phi}$:

$$s = 4\,\bar{\Phi}_{z\bar{z}} - i\delta(z-\bar{z}) \tag{IV.46}$$

$$t = -2\frac{\bar{z}}{z}\,\bar{\Phi}_{\bar{z}\bar{z}} \tag{IV.47}$$

After transformation, Hooke's Law becomes

$$s(1-2\nu) = 2\mu\left[\left(\frac{u_z}{\sqrt{z\bar{z}}}\right)_z + \left(\frac{u_{\bar{z}}}{\sqrt{z\bar{z}}}\right)_{\bar{z}}\right] \tag{IV.48}$$

$$t = 2\mu\,\bar{z}\left(\frac{u}{\sqrt{z\bar{z}}}\right)_{\bar{z}} \tag{IV.49}$$

Again two complex equations replace the four equations in real coordinates which relate σ_r, σ_θ, σ_z, τ_{rz} to u_r and u_θ. Since (IV.48) and (IV.49) are related through $\bar{\Phi}$, it follows that the displacements u must be made compatible with the space spanned by the generating function. Elimination of u between (IV.48) and (IV.49) yields with the help of (IV.46) and (IV.47):

$$\bar{\Phi}_{zz\bar{z}\bar{z}} = 0 \tag{IV.50}$$

This equation may be integrated in the complex domain to yield:

$$2\bar{\Phi} = \bar{z}f + z\bar{f} + g + \bar{g} \tag{IV.51}$$

where f and g are two arbitrary functions which depend only on the one complex variable z. Likewise the conjugate functions $\bar{f}$, $\bar{g}$ depend only on the conjugate variable $\bar{z}$. Introducing (IV.51) into (IV.46), (IV.47), (IV.48) and (IV.49) yields after integration:

$$2\mu u = (3-4\nu)\sqrt{\frac{\bar{z}}{z}}\,f - \sqrt{z\bar{z}}\,\bar{f}_{\bar{z}} - \sqrt{\frac{\bar{z}}{z}}\,\bar{g}_{\bar{z}} - \frac{i\delta}{2}(1-2\nu)z\sqrt{z\bar{z}} + iC\sqrt{z\bar{z}} + B\sqrt{\frac{\bar{z}}{z}} \tag{IV.52}$$

$$s = 2f_z + 2\bar{f}_{\bar{z}} - i\delta(z - \bar{z}) \tag{IV.53}$$

$$t = -\bar{z}\,\bar{f}_{\bar{z}\bar{z}} - \frac{\bar{z}}{z}\,\bar{g}_{\bar{z}\bar{z}} \tag{IV.54}$$

where C and B are arbitrary constants and represent rigid body motions respectively due to rotation and translation.

At the inner boundary of the circular ring (r = a) both the radial and shear stressses are zero, so that

$$\sigma_r + i\tau_{r\theta} = \frac{s}{2} + t = 0 \tag{IV.55}$$

At the propellant-rigid case interface there is no displacement so that:

$$u_r + i u_\theta = u = 0, \quad \text{at} \quad r = b \tag{IV.56}$$

In a multiply connected region, perforated by one hole, it is readily shown* that the complex potentials f and g_z are given by:

$$f = A \ln z + \sum_{-\infty}^{\infty} a_k z^k \tag{IV.57}$$

$$g_z = (3 - 4\nu) A \ln z + \sum_{-\infty}^{\infty} a'_k z^k \tag{IV.58}$$

where the coefficients A, a_k, a'_k are to be determined from conditions (IV.55), (IV.56). Muskhelishvili has shown that f and g_z are holomorphic in a simply connected domain and therefore are capable of power series representation of the type used in (IV.57) and (IV.58). Convergence is guaranteed by scaling the modulus of z to the radius of a unit circle. Substituting (IV.57) and (IV.58) into (IV.55) and (IV.56) and equating coefficients yields the complete solution in a perfectly straightforward manner:

$$f = A + B \ln z + C z^2 \tag{IV.59}$$

* Muskhelishvili, N. I., Material Theory of Elasticity, p. 218, Noordhoff (1953).

$$g_z = D + B(3-4\nu)\ln z + \frac{F}{z^2} \tag{IV.60}$$

$$B = -\frac{i\delta a^2}{8(1-\nu)} \tag{IV.61}$$

$$C = \frac{i\delta\left[a^2b^2 + a^4(1-2\nu) + 4b^4(1-\nu)(1-2\nu)\right]}{8(1-\nu)\left[a^4 + b^4(3-4\nu)\right]} \tag{IV.62}$$

$$F = \frac{i\delta a^4 b^2\left[a^2 + b^2(1-2\nu)\right]}{8(1-\nu)\left[a^4 + b^4(3-4\nu)\right]} \tag{IV.63}$$

$$(3-4\nu)A - \bar{D} = \frac{(3-4\nu)\,i\delta a^2 \ln b}{4(1-\nu)} - \frac{2b^2 i\delta\left[a^2b^2 + a^4(1-2\nu) + 4b^4(1-\nu)(1-2\nu)\right]}{8(1-\nu)\left[a^4 + b^4(3-4\nu)\right]} \tag{IV.64}$$

Note that in (IV.64), A and D are related. Since these coefficients separately represent rigid body motions, it is impossible to separate them without introducing an arbitrary assumption about one or the other. However, only the difference $(3-4\nu)A - \bar{D}$ contributes to the displacement field as evaluated by equation (IV.47), so that it is unnecessary to introduce any further conditions to determine A or D.

By substituting (IV.59) - (IV.64) into (IV.52) - (IV.54), one obtains the complete solution to the assumed slump problem. This complex solution in turn can be separated into real and imaginary parts and cast in terms of real variables. After doing this and evaluating the displacements at a and the stresses at b, one obtains

$$\frac{\tau_{r\theta}(b)}{\delta b} = \frac{a_f\left[(2-a_f)(1-a_f) + 2(1-2\nu)\right]}{2\left[(1-a_f)^2 + (3-4\nu)\right]}\cos\theta \tag{IV.66}$$

$$\frac{\sigma_r(b)}{\delta b} = \frac{a_f\left[(1-\nu) - a_f(1-a_f)\right]}{2\left[(1-a_f)^2 + (3-4\nu)\right]}\sin\theta \tag{IV.67}$$

$$\frac{-2\mu u_r(a)}{\delta b^2} = \left\{ \frac{(3-4\nu)(1-a_f)\ln(1-a_f)}{8(1-\nu)} + a_f \frac{[(1-a_f)^2(2-3\nu)+\nu(1-a_f)+4(1-\nu)(1-2\nu)]}{4(1-\nu)[(1-a_f)^2+(3-4\nu)]} \right\} \sin\theta \quad \text{(IV.68)}$$

$$\frac{-2\mu u_\theta(a)}{\delta b^2} = \left\{ \frac{(3-4\nu)(1-a_f)\ln(1-a_f)}{8(1-\nu)} + a_f \frac{[4(1-\nu)(1-2\nu)+(2-\nu)(1-a_f)-\nu(1-a_f)^2]}{4(1-\nu)[(1-a_f)^2+(3-4\nu)]} \right\} \cos\theta \quad \text{(IV.69)}$$

where in (IV.68) $a_f = 1 - \frac{a^2}{b^2}$ is the volume fraction of loading of the case based on cross-sectional dimensions.

Taking $\nu = 1/2$, $a_f = .80$, we obtain for the maximum values of the stresses and displacements

$$\tau_{r\theta}(\text{on } b \text{ @ } \theta = 0) = 0.092\ \delta b \quad \text{(IV.70)}$$

$$\sigma_r\left(\text{on } b \text{ @ } \theta = \frac{\pi}{2}\right) = 0.708\ \delta b \quad \text{(IV.71)}$$

$$2\mu \frac{u_r}{a}\left(\text{on } a \text{ @ } \theta = \frac{\pi}{2}\right) = 0.345\ \delta a \quad \text{(IV.72)}$$

$$2\mu \frac{u_\theta}{a}(\text{on } a \text{ @ } \theta = 0) = -0.140\ \delta a \quad \text{(IV.73)}$$

with $b = 160''$, $a = 71.6''$, and $\delta = .0625$ lbf/cu in, we obtain:

$$\tau_{r\theta} \text{ (max on b)} = 0.92 \text{ psi} \quad \text{(IV.74)}$$

$$\sigma_r \text{ (max on b)} = 7.08 \text{ psi} \quad \text{(IV.75)}$$

$$2\mu \frac{u_r}{a} \text{ (max on a)} = 1.54 \text{ psi} \quad \text{(IV.76)}$$

$$2\mu \frac{u_\theta}{a} \text{ (max on a)} = -0.65 \text{ psi} \quad \text{(IV.77)}$$

For $\mu = 200$ psi, it is observed that the maximum strain due to horizontal

slump will not exceed a few tenths per cent. Likewise the stresses at the propellant-liner interface are negligible. It is concluded that uniform horizontal slump is of no consequence in large motors.

C. MIXED BOUNDARY VALUE PROBLEM OF A FINITE RECTANGLE

The first three progress reports in this series have presented in this section on Stress Analysis a thorough discussion of the stress-displacement field in the vicinity of a geometrical discontinuity. Two types of analysis were used--a transform technique and an eigenvalue method. The former gives the complete solution along divergent boundaries and also allows one to identify a given path of integration with a given set of surface tractions. The latter gives solutions for unbounded problems which are valid in the limit of zero surface tractions and displacements and for bounded problems only in the neighborhood of the geometric discontinuity. It generates a set of eigenvalues which has not yet been proved to be complete, and which may, under special types of loading, not contribute significantly to the particular solution of the bounded problem. Despite these limitations, the method has met with success as is shown in a previous paragraph of this section.

The first application of these techniques was to simple geometries characterized by a single geometric discontinuity--the wedge, the cylinder in axial compression, and the cylinder in radial compression. In the latter two problems, an approximation was made to obtain the solutions near the edge singularity. Thus, apart from the almost trivial problems of the wedge, there has not been generated a complete solution to a body with finite boundaries. This immediately implies two or more edges and concatenately, two or more points of singularity.

In order to pursue this point more fully, we are currently investigating the simplest finite body--the infinite rectangular slab. This is the limiting case of a very long bar and generates the simplest plane-strain solution for a body with two points of singularity. This problem has already been tackled by mapping the rectangle into a sphere. In the course of our investigation of mapping techniques it occurred that a method could be developed in which complex variable techniques were applied directly to a rectangle without mapping. An advantage accrues

in preserving the relatively simple boundary conditions. On the other hand, complexity arises in determining the coefficients of the Fourier expansions. A method for obviating this complexity is developed in the succeeding paragraphs.

In the sketch below the rectangular cross-section of the bar is geometrized on the complex plane, with the compressed elements shown as bowed arcs. The domain of the rectangle is a sub-domain of the unit-circle , with $b < a$.

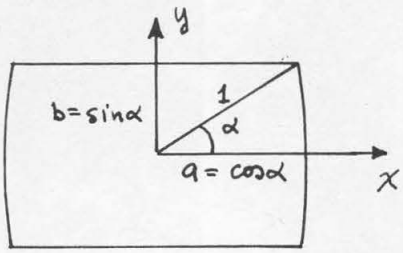

$$\text{on } x=a,\ \sigma_x = \tau_{xy} = 0 \tag{IV.77}$$

$$\text{on } y=b,\ u_x = \frac{\partial u_y}{\partial x} = 0 \tag{IV.78}$$

$$\text{on } x=0,\ \frac{\partial \sigma_y}{\partial x} = \frac{\partial u_y}{\partial x} = u_x = \tau_{xy} = 0 \tag{IV.79}$$

$$\text{on } y=0,\ \tau_{xy} = u_y = \frac{\partial u_x}{\partial y} = \frac{\partial \sigma_x}{\partial y} = 0 \tag{IV.80}$$

The problem is to compute $P = \int_{-a}^{a} \sigma_y \big|_{y=b} dx$ as a function of $S = \frac{u_y}{b}\big|_{y=b}$

Introducing complex stresses and displacements we have:

$$\sigma_x + \sigma_y = s \tag{IV.81}$$

$$\frac{\sigma_x - \sigma_y}{2} + i\tau_{xy} = t \tag{IV.82}$$

$$u_x + i u_y = u \tag{IV.83}$$

These quantities in turn can be generated from two complex potentials, which are holomorphic functions all over the rectangle except possibly at the four corners.

$$2\mu u = (3-4\nu) f - z\bar{f}_{\bar{z}} - \bar{g}_{\bar{z}} \tag{IV.84}$$

$$\frac{s}{2} = f_z + \bar{f}_{\bar{z}} \tag{IV.85}$$

$$-t = z f_{\bar{z}\bar{z}} + \bar{g}_{\bar{z}\bar{z}} \tag{IV.86}$$

$$f = \sum_0^\infty a_k z^k \tag{IV.87}$$

$$g_z = \sum_0^\infty b_k z^k \tag{IV.88}$$

In (IV.87) and (IV.88) the Fourier coefficients a_k and b_k are to be interpreted as complex constants. These must be determined by introducing (IV.87), and (IV.88) into (IV.84), (IV.85), and (IV.86) with the boundary condition:

$$\text{on } \bar{\zeta} = -\zeta \pm 2\cos\alpha, \quad \frac{s}{2} + \bar{t} = 0, \text{ and } t = \bar{t} \tag{IV.89}$$

$$\text{on } \bar{\zeta} = \zeta \pm 2i\sin\alpha, \quad \bar{u} + u = u_\zeta + u_{\bar{\zeta}} = 0 \tag{IV.90}$$

$$\text{on } \bar{\zeta} = +\zeta, \quad t = \bar{t} \quad \text{and} \quad u = \bar{u} \tag{IV.91}$$

$$\text{on } \bar{\zeta} = -\zeta, \quad t = \bar{t} \quad \text{and} \quad u = \bar{u} \tag{IV.92}$$

Substitution into (IV.89) yields the pair of equations:

$$\sum_0^\infty k a_k \zeta^{k-1} + \sum_0^\infty k \bar{a}_k \bar{\zeta}^{k-1} = \bar{\zeta} \sum_0^\infty k(k-1) a_k \zeta^{k-2} + \sum_0^\infty k b_k \zeta^{k-1} \tag{IV.93}$$

$$\bar{\zeta} \sum_0^\infty k(k-1) a_k \zeta^{k-2} + \sum_0^\infty k b_k \zeta^{k-1} = \zeta \sum_0^\infty k(k-1) \bar{a}_k \bar{\zeta}^{k-2} + \sum_0^\infty k \bar{b}_k \bar{\zeta}^{k-1}$$

The first of these can be rewritten:

$$\sum_1^\infty k a_k \zeta^{k-1} + \sum_1^\infty k \bar{a}_k (-\zeta \pm 2\cos\alpha)^{k-1} = (-\zeta \pm 2\cos\alpha) \sum_2^\infty k(k-1) a_k \zeta^{k-2} + \sum_1^\infty k b_k \zeta^{k-1} \tag{IV.94}$$

We now expand all the powers of all the trigonometric binomials:

$$\text{e.g., } (\pm 2\cos\alpha - \zeta)^m = \sum_{s=0}^m \binom{m}{s} (\pm 2\cos\alpha)^s (-\zeta)^{m-s} \tag{IV.95}$$

Similar substitutions and expansions obtain for eqs. (IV.90), (IV.91), and (IV.92). The coefficients of ζ can then be lumped and equated. This leads to a doubly infinite set of matrices for the sets $\{a_k\}$ and $\{b_k\}$. Special techniques of Hilbert space are being used to convert these matrices. The results of this solution will be presented in the succeeding progress report.

After carrying out these expansions in the domain of the quarter rectangle the center of which has been mapped onto the origin of the

complex plane, some consideration must be given to the rate of convergence of the series. This should be rapid throughout most of the domain except in the neighborhood of the vertex of the rectangle which lies on the unit circle. In order to investigate the solution at this point, it is convenient to map this point onto the origin of the complex plane, and map the center of the rectangle onto the unit circle. This should make for rapid convergence throughout the entire domain of the quarter-rectangle. This approach will also be presented in the succeeding progress report.